University of Reading

Wind pressure on a single building immersed in a low-jet wind profile

Conference or Workshop Item

Accepted Version

Luo, Z. and Hang, J. (2013) Wind pressure on a single building immersed in a low-jet wind profile. In: International Conference of SuDBE2013, 25-28 Oct 2013, Chongqing, China. Available at http://centaur.reading.ac.uk/36698/

It is advisable to refer to the publisher's version if you intend to cite from the work. See Guidance on citing.

All outputs in CentAUR are protected by Intellectual Property Rights law, including copyright law. Copyright and IPR is retained by the creators or other copyright holders. Terms and conditions for use of this material are defined in the End User Agreement.

www.reading.ac.uk/centaur

University of Reading

CentAUR

Central Archive at the University of Reading

Reading's research outputs online

Wind pressure on a single building immersed in a low-jet wind profile

Zhiwen Luo[1,2], Jian Hang[3]

(1. Key laboratory of the Three Gorges Reservoir Region's Eco-Environment, Ministry of Education, Chongqing University, Chongqing, China
(2. School of Construction Management and Engineering, University of Reading, United Kingdom
(3. Department of Atmospheric Sciences, School of Environmental Science and Engineering of Sun Yat-Sen University, Guangzhou, P. R. China)

Abstract: This paper for the first time discuss the wind pressure distribution on the building surface immersed in wind profile of low-level jet rather than a logarithmic boundary-layer profile. Two types of building models are considered, low-rise and high-rise building, relative to the low-level jet height. CFD simulation is carried out. The simulation results show that the wind pressure distribution immersed in a low-jet wine profile is very different from the typical uniform and boundary-layer flow. For the low-rise building, the stagnation point is located at the upper level of windward façade for the low-level jet wind case, and the separation zone above the roof top is not as obvious as the uniform case. For the high-rise building model, the height of stagnation point is almost as high as the low-level jet height.

Key words: wind pressure, low-jet profile, building ventilation

1 Introduction

The knowledge of wind pressure on the building façade is vital for the wind loading engineering and infiltration and ventilation studies [1-2]. It is also one of the important input parameters for building energy simulation (BES) program and multi-zone airflow program [3].

Values of the mean local wind pressure coefficient depend on many factors, including the size and shape of the building [2], approaching wind profile [4-5], the location and proximity of neighboring buildings [6], vegetation [7], and terrain features[8]. Different approaches such as wind tunnel, CFD, on-site field measurement are usually employed [9]. However, almost all the studies assume approaching wind flow to be of an atmospheric boundary layer (ABL) profile, represented by a power law or logarithmic law [10-13]. Therefore, the wind speed increases exponentially with the height. Nevertheless, we are asking the following question:

-What are the characteristics of wind pressure (coefficient) and its resultant ventilation rate when the building is not exposed to a conventional ABL but a low-level jet profile?

Slope wind characterized by a low-level jet is a local wind system frequently observed in mountainous areas under a calm and cloud-free synoptic weather condition[14]. The driving force is the natural convection induced by a temperature difference between mountain slope and ambient air temperature [15-16].Two types of slope wind can be distinguished due to its opposite thermal forcing. In the daytime, upslope (anabatic) wind is developed when the slope surface is heated up by the solar radiation, and the radiative cooling to the sky will lead to a downslope (katabatic) flow from the mountain slope at nighttime [17]. The slope wind exhibits a low-level jet profile, characterized by a maximum velocity close to the ground surface. Recently, many efforts have been made to investigate the ventilation of urban built-up environment by slope winds [18-20] ,however, no study has been found to link the slope flow with building-scale ventilation, to our best knowledge. The wind pressure characteristics on building façades and its resultant cross-ventilate rate induced by slope winds are lacking.

2 Slope wind: low-jet profile

Consider an infinite mountain slope inclines by an angle of α to the horizontal, which everywhere has a definite excess of temperature over the stratified mass of air. The Cartesian coordinate system is set as s in the direction of along the slope surface, and n normal to the slope. The Coriolis force is neglected. The one-dimensional governing equations of thermally-driven katabatic slope wind are given by considering the balance

between the buoyancy force and turbulent divergence, as follows

$$\begin{cases} g\beta\Delta\theta\sin\alpha = k_m \dfrac{d^2u(n)}{dn^2} \\ -\gamma u(n)\sin\alpha = k_h \dfrac{d^2\Delta\theta}{dn^2} \end{cases} \quad (1)$$

Where $\Delta\theta$ is the potential temperature perturbation along the slope surface from the free atmosphere at the same height; N is the Brunt-Vaisala frequency; k_m is momentum eddy diffusivity, k_h is thermal eddy diffusivity, γ is lapse rate, β is thermal expansion coefficient.

The general solution of Eq.(1) is obtained

$$\begin{cases} u(n) = \dfrac{g\beta\Delta\theta_s}{N}\exp(-\dfrac{n}{l})\sin\dfrac{n}{l} \\ \Delta\theta(n) = \Delta\theta_s\exp(-\dfrac{n}{l})\cos\dfrac{n}{l} \end{cases} \quad (2)$$

Where $l = \sqrt[4]{\frac{4k_m k_h}{g\beta\gamma\sin^2(\alpha)}}$ is a length scale; $\Delta\theta_s$ is the temperature deficit at the slope surface. The height of the wind maxima occurs at the height of h_{max}

$$h_{max} = \frac{\pi}{4}l \quad (3)$$

The example of velocity profile can be seen in Fig.1, red solid line. The maximum velocity for the slope wind is 4.61 m/s at a height of around 56 m. The input parameters for calculation are listed in Table1. Another two types of approaching wind profiles: a uniform flow with a constant velocity of 4.61 m/s at all heights and a boundary layer flow characterized by Eq.(4) are also considered for comparison. z_{ref} is reference height, which is defined at building height. Two building models (w × w × h) are adopted based on their relative heights to the slope wind jet height. *w*=20m is the building width, keeping the same for all three cases. *h* is building height. *h*=*w* is a low-rise building with a height much lower than slope wind height, and *h*=5*w* represents a high-rise building with a height much higher than slope wind height, respectively.

$$\frac{u}{u_{ref}} = \left(\frac{z}{z_{ref}}\right)^{0.15} \quad (4)$$

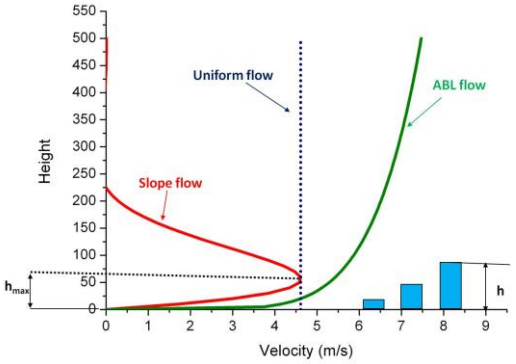

Fig.1 Different approaching wind profiles

Table 1 Input parameters for slope wind

Temperature difference between slope surface and ambient temperature, $\Delta\theta_s$ (°C)	**-5**
Coefficient of thermal expansion, β (1/K)	1/298
Background lapse rate, γ (K/m)	0.004
Buoyancy frequency, N (1/s)	0.0115
Thermal eddy diffusivity, k_h	10
Momentum eddy diffusivity, k_m	10

3 CFD simulation and validation

3.1 CFD setup

A 1:100 reduced computational model was made to compare against the wind

tunnel measurement. The computational domain was set as L*D*H = 53h*25h*12.5h, which is much higher than the recommendation from the best practice guideline from Franke et al [21]and Tominaga et al[22-23] except the upstream distance. In modeling the external airflow in the ABL, horizontal homogeneity is always required [10, 24-25]. We adopted an upstream distance of 3h rather than 5h to make little variation of velocity magnitude along the wind direction before it reaches the building block. This choice of upstream distance can be also found in [26-27]. A relatively low turbulent intensity of 10% was also implemented at the inlet boundary for all three approaching flow profiles to reduce the momentum transfer towards the ground and therefore improve the horizontal homogeneity of the approaching flow. This value corresponds to the typical turbulence intensity range in the nocturnal boundary layer. The turbulent kinetic energy and dissipate rate are calculated as follows (Yang et al, 2008)

$$k(z) = (I_u(z)u(z))^2$$

$$\varepsilon(z) = C_\mu^{0.75} k^{1.5}/(Kz)$$

As a matter of fact, the turbulence characteristics of the three approaching profiles are different, but this difference is beyond the scope of present study as our focus is the average wind profile. The mean velocity at the inlet boundary is calculated based Eq.(2) and Eq.(4). Zero static pressure boundary condition is imposed at the outlet plane and symmetry boundary conditions with zero normal velocity and gradients of all variables are applied at the top and lateral sides. RNG k-ε turbulence model is employed to take care of the turbulence modeling.

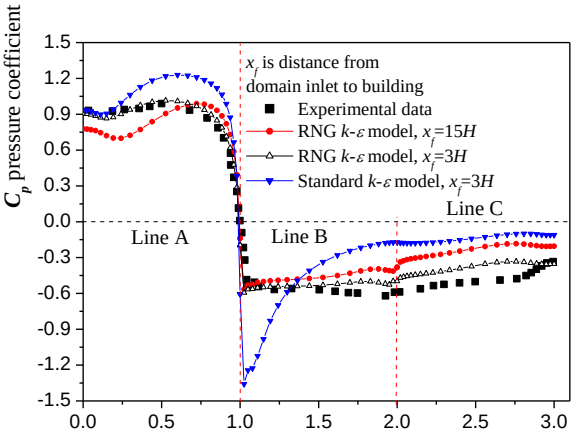

Fig.2 Comparison of CFD simulation and wind tunnel data for validation case

3.2 Validation with wind tunnel experiment

The validation case follows the wind tunnel experiment carried out by [28].

Two types of turbulence model, i.e., standard and RNG k-ε are compared. It shows that standard k-ε over estimates the wind pressure at the roof level, while RNG turbulent model gives a relatively reasonable estimation. Later on, two upstream domain lengths are also considered, 15H and 3H. The conclusion is that Xf =3H can better reproduce the Cp value compared with the longer upstream length as it reduces the stream-wise inhomogeneity along the domain, see Fig.2.

4 Results and discussion

4.1 Low-rise building

Fig.3 shows the velocity vector on the middle plane across the building façade for two types of approaching profiles. The most significant difference between the two approaching wind profiles locates at the roof level. For the uniform incoming wind, an obvious separation zone is located just above the roof top, accompanied by a dramatic increase of wind speed at leading separation edge. While for low-level jet case, such separation zone is not well formed. This is partly due to a relatively low wind speed at the roof level of the building. At leeward side, the well-presented recirculation zone in the case of uniform approaching wind is not observed in the low-level jet case. For the wind pressure distribution on the windward façade, the location of stagnation point is much higher in low-level jet wind case than in the uniform wind. It is well accepted that the stagnation point in a boundary layer flow is located at 2/3 of the windward face height. This height is still lower than our case in a low-level jet profile. This unique stagnation point location corresponds to the wind vector distribution in front of the windward façade, as shown in Fig.3 a) and b), where the location of flow divergence occurs much higher in the low-lower jet wind compared with uniform wind.

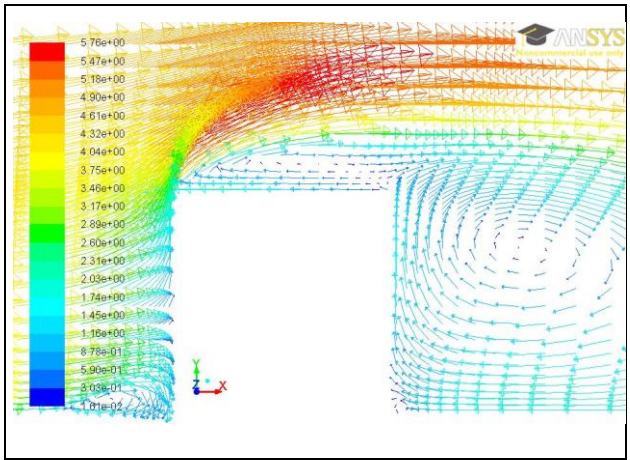

a)

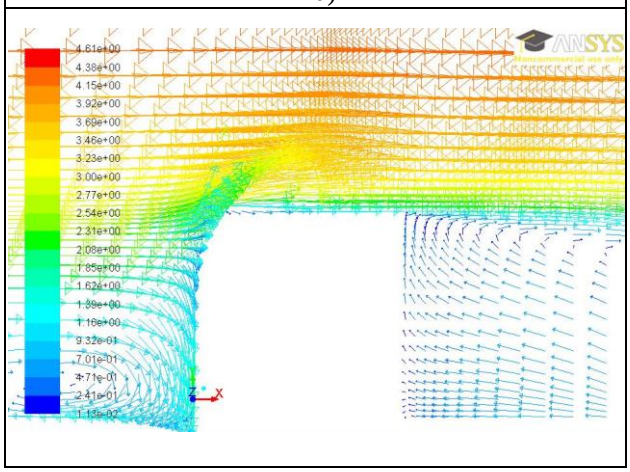

b)

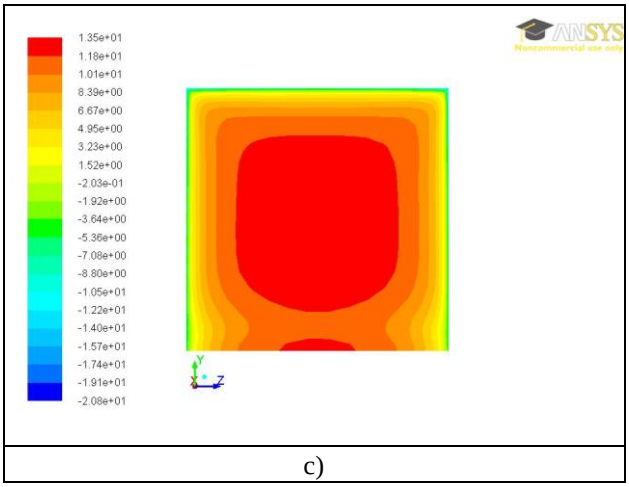

c)

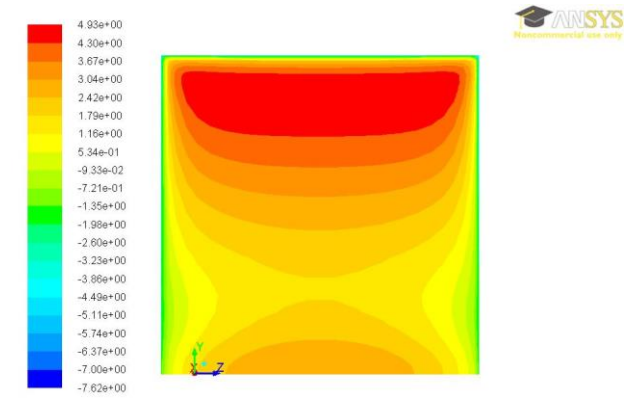

d)

Fig.3 Velocity vector across the low-rise building middle plane, a) uniform profile, b) low-level jet profile; Wind pressure distribution at windward façade, c) uniform profile, d) low-level jet profile

4.2 High-rise building

For a high-rise building, the building height is comparable to the low-level jet height. The wind pressure at the windward façade for the low-level jet wind is different from the low-rise building. The stagnation point is not located at the upper level of the façade, but corresponding to the jet height, where the maximum velocity locates. For the uniform case, the surface wind pressure is quite uniform, as shown in Fig.4. c) and d).

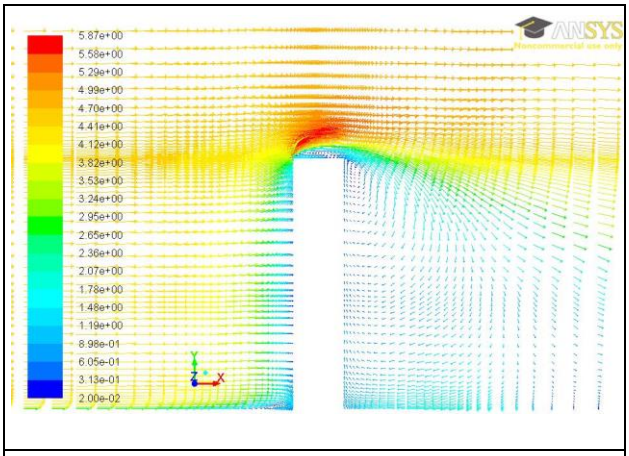

b)

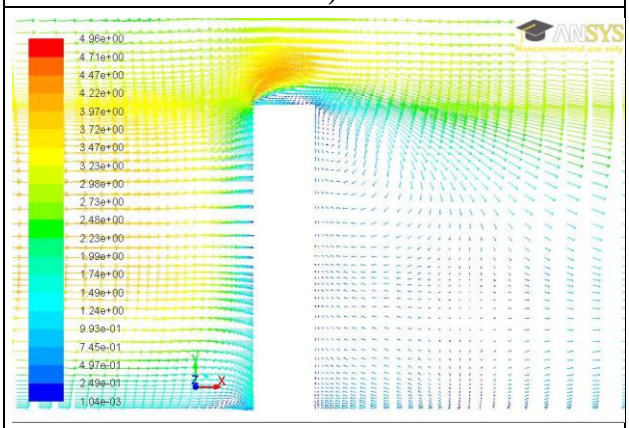

b)

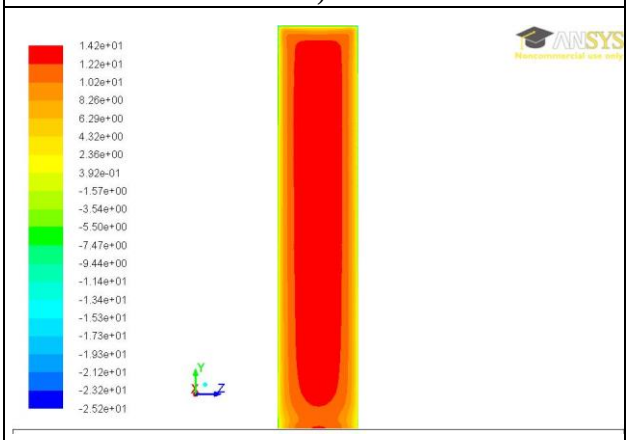

c)

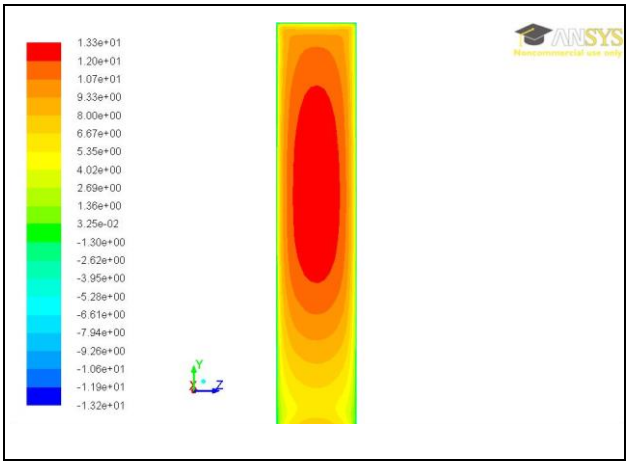

d)

Fig.4 Velocity vector across high-rise building middle plane, a) uniform profile, b) low-level jet profile; Wind pressure distribution at windward façade, c) uniform profile, d) low-level jet profile

5 Conclusions

The paper presents the comparative study of wind pressure distribution for a building model immersed in different approaching wind profiles, i.e., uniform wind and a typical low-level jet profile by CFD simulation. The simulation results show that the wind pressure distribution immersed in a low-jet wine profile is very different from the typical uniform and boundary-layer flow. For the low-rise building, the stagnation point is located at the upper level of windward façade for the low-level jet wind case, and the separation zone above the roof top is not as obvious as the uniform case. For the high-rise building model, the height of stagnation point is almost as high as the low-level jet height.

References

[1] Montazeri H, Blocken B. CFD simulation of wind-induced pressure coefficients on buildings with and without balconies: Validation and sensitivity analysis. Building and Environment. 2013;60:137-49.

[2] Uematsu Y, Isyumov N. Wind pressures acting on low-rise buildings. Journal of Wind Engineering and Industrial Aerodynamics. 1999;82:1-25.

[3] Cóstola D, Blocken B, Hensen JLM. Overview of pressure coefficient data in building energy simulation and airflow network programs. Building and Environment. 2009;44:2027-36.

[4] Yang W, Quan Y, Jin X, Tamura Y, Gu M. Influences of equilibrium atmosphere boundary layer and turbulence parameter on wind loads of low-rise buildings. Journal of Wind Engineering and Industrial Aerodynamics. 2008;96:2080-92.

[5] Köse DA, Fauconnier D, Dick E. ILES of flow over low-rise buildings: Influence of inflow conditions on the quality of the mean pressure distribution prediction. Journal of Wind Engineering and Industrial Aerodynamics. 2011;99:1056-68.

[6] Pindado S, Meseguer J, Franchini S. Influence of an upstream building on the wind-induced mean suction on the flat roof of a low-rise building. Journal of Wind Engineering and Industrial Aerodynamics. 2011;99:889-93.

[7] Stathopoulos T, Chiovitti D, Dodaro L. Wind shielding effects of trees on low buildings. Building and Environment. 1994;29:141-50.

[8] Maier-Erbacher J, Plate EJ. Measurement of velocity near and pressure on a cylindrical tower located on irregular terrain. Journal of Wind Engineering and Industrial Aerodynamics. 1991;38:167-84.

[9] El-Okda YM, Ragab SA, Hajj MR. Large-eddy simulation of flow over a surface-mounted prism using a high-order finite-difference scheme. Journal of Wind Engineering and Industrial Aerodynamics. 2008;96:900-12.

[10] Blocken B, Stathopoulos T, Carmeliet J. CFD simulation of the atmospheric boundary layer: wall function problems. Atmospheric Environment. 2007;41:238-52.

[11] Fang C, Sill BL. Pressure distribution on a low-rise building model subjected to a family of boundary layers. Journal of Wind Engineering and Industrial Aerodynamics. 1995;56:87-105.

[12] Wieringa J. Updating the Davenport roughness classification. Journal of Wind Engineering and Industrial Aerodynamics. 1992;41:357-68.

[13] Stathopoulos T. Computational wind engineering: Past achievements and future challenges. Journal of Wind Engineering and Industrial Aerodynamics. 1997;67–68:509-32.

[14] Ye ZJ, Segal M, Pielke RA. Effects of Atmospheric Thermal Stability and Slope Steepness on the Development of Daytime Thermally Induced Upslope Flow. Journal of the Atmospheric Sciences. 1987;44:3341-54.

[15] Whiteman CD. Mountain Meteorology: Fundamental and Applications. New York Oxford University Press; 2000.

[16] Yi C, Monson RK, Zhai Z, Anderson DE, Lamb B, Allwine G, et al. Modeling and measuring the nocturnal drainage flow in a high-elevation, subalpine forest with complex terrain. Journal of Geographical Research. 2005;110,D22303, doi:10.1029/2005JD006282.

[17] Kitada T, Okamura K, Tanaka S. Effects of Topography and Urbanization on Local Winds and Thermal Environment in the Nohbi Plain, Coastal Region of Central Japan: A Numerical Analysis by Mesoscale Meteorological Model with a k-epsilon Turbulence Model. Journal of

Applied Meteorology. 1998;37:1026-46.

[18] Luo Z, Li Y. Passive urban ventilation by combined buoyancy-driven slope flow and wall flow: Parametric CFD studies on idealized city models. Atmospheric Environment. 2011;45:5946-56.

[19] Yang L, Li Y. City ventilation of Hong Kong at no-wind conditions. Atmospheric Environment. 2009;43:3111-21.

[20] Kuttler W, Barlag A-B, Robmann F. Study of the thermal structure of a town in a narrow valley. Atmospheric Environment. 1996;30:365-78.

[21] Franke J, Hellsten A, Schlunzen H, Carrissimo B. Best practice guideline for the CFD simulation of flows in the urban environment. Brussels: COST Office; 2007.

[22] Tamura T, Nozawa K, Kondo K. AIJ guide for numerical prediction of wind loads on buildings. Journal of Wind Engineering and Industrial Aerodynamics. 2008;96:1974-84.

[23] Tominaga Y, Mochida A, Yoshie R, Kataoka H, Nozu T, Yoshikawa M, et al. AIJ guidelines for practical applications of CFD to pedestrian wind environment around buildings. Journal of Wind Engineering and Industrial Aerodynamics. 2008;96:1749-61.

[24] Gorlé C, van Beeck J, Rambaud P, Van Tendeloo G. CFD modelling of small particle dispersion: The influence of the turbulence kinetic energy in the atmospheric boundary layer. Atmospheric Environment. 2009;43:673-81.

[25] Richards PJ, Norris SE. Appropriate boundary conditions for computational wind engineering models revisited. Journal of Wind Engineering and Industrial Aerodynamics. 2011;99:257-66.

[26] Köse DA, Dick E. Prediction of the pressure distribution on a cubical building with implicit LES. Journal of Wind Engineering and Industrial Aerodynamics. 2010;98:628-49.

[27] Ramponi R, Blocken B. CFD simulation of cross-ventilation flow for different isolated building configurations: Validation with wind tunnel measurements and analysis of physical and numerical diffusion effects. Journal of Wind Engineering and Industrial Aerodynamics. 2012;104–106:408-18.

[28] Castro IP, Robins AG. The flow around a surface-mounted cube in uniform and turbulent streams. Journal of Fluid Mechanics. 1977;79:307-35.